Peer-reviewed version available at *Energies* **2020**, *13*, 1196; doi:10.3390/en13051196

Type of the Paper (Article)

Pore-Fractures of Coalbed Methane Reservoir Restricted by Coal Facies in Sanjiang-Mulinghe Coal-Bearing Basins, Northeast China

Yuejian Lu [1,2], Dameng Liu [1,2,*], Yidong Cai [1,2], Qian Li[1,2] and Qifeng Jia [1,2]

[1] School of Energy Resources, China University of Geosciences, Beijing 100083, PR China; 3006180024@cugb.edu.cn (Y.L.); yidong.cai@cugb.edu.cn (Y.C.); li.qian@cugb.edu.cn (Q.L.); 3006190029@cugb.edu.cn (Q,J.)

[2] Coal Reservoir Laboratory of National Engineering Research Center of Coalbed Methane Development & Utilization, Beijing 100083, PR China

* Correspondence: dmliu@cugb.edu.cn; Tel.: +86-10-82323971

Abstract: Pore-fractures network play a key role in coalbed methane (CBM) accumulation and production, while the impacts of coal facies on the pore-fractures network performance are still poorly understood. In this work, the research on the pore-fracture occurrence of 38 collected coals from Sangjiang-Muling coal-bearing basins with multiple techniques including mercury intrusion porosimetry (MIP), micro-organic quantitative analysis, and optic microscopy, and its variation controlling of coal face were studied. The MIP curves of 38 selected coals indicating pore structures were subdivided into three typical types including type I of predominant micropores, type Ⅱ of predominant micropores and macropores with good connectivity and type Ⅲ of predominant micropores and macropores with poor connectivity. For coal facies, there are three various coal facies were distinguished, which include lake shore coastal wet forest swamp, the upper delta plain wet forest swamp, tidal flat wet forest swamp with Q-cluster analysis and tissue preservation index - gelification index (TPI-GI) and Wood index - groundwater influence index (WI -GWI). The results show there is positive relationship between tissue preservation index (TPI), wood index (WI) and mesopores (10^2nm-10^3nm), while a negative relationship between TPI, WI and macropores/fractures. In addition, groundwater level fluctuations can control the development of type C and D fractures, and the frequency of type C and D fractures shows an ascending trend with increasing GWI, which may be caused by the mineral hydration of the coal. Finally, from the perspective of the pore-fractures occurrence in CBM reservoirs, the wet forest swamp of upper delta plain is considered to be the optimization areas for Sanjiang-Mulinghe coal-bearing basins by a comparative study of various coal facies.

Keywords: Pore-fracture network, Coal facies, Coalbed methane reservoir, Sangjiang-Muling basin

Peer-reviewed version available at Energies 2020, 13, 1196; doi:10.3390/en13051196

1. Introduction

Coal is the source rock and reservoir for coalbed methane (CBM) [1]. The growing emphasis on CBM in many countries including China, United States and Australia recent years since its beneficial to safety production of mine, greenhouse gas reduction and great economic value as a form of clean unconventional natural gas resource[2-6]. Currently, high costs and low production rate are two key factors influencing CBM commercial development [7]. The dual pore-fracture system of CBM reservoir can provide CBM enrichment space and the channel for the gas adsorption, diffusion and seepage. The fracture is made up of micro-fracture and macro-fracture, the former is the bridge of pores and macro-fractures, macro-fracture is the pathway for CBM flow from coal reservoirs to wellbores [8-10]. Hence, evaluating pore-fracture is important to acquire high abundance CBM reservoir and high productivity reservoir.

Discrepancy in pore-fracture characteristics caused the different CBM reservoir permeability, porosity, and the capacity of gas adsorption. In this work, the combined pore size classification will be adopted, which is classified as micropores (<10 nm), transition pores (10 nm - 10^2 nm), mesopore (10^2 nm - 10^3nm), macropores (10^3 nm - 10^4 nm), and super pores/microfractures (over 10^4 nm) [11,12], the content of micropores and transition pores represent adsorption capacity of CBM in the coal reservoir, the higher the proportion of micropores and transition pores, the stronger adsorption capacity [12]. Pore-fracture may also greatly affect the interaction between pore-fracture and gas-liquid molecules. Micropores and mesopores has great affinity with certain gases (e.g., CO_2, CH_4,) because of its extremely large internal surface area and large quantities of gas is adsorbed on the surface of pore in the adsorbed state[12–14]. Pervious scholars suggested that the matrix permeability is controlled by pore size distribution and the connectivity between pores and fractures, N_2 BET surface area should be influenced by the mesopores structure [15,16]. For natural fractural factures, the hydraulic fracturing is an effective way to enhance CBM recovery by increasing the width and length of the natural fractures and improving the connectivity among the natural fractures [17,18].

Factors influencing pore-fracture of CBM reservoir through the coalification on pore-fracture characteristics has been limited investigated by using MIP and gas adsorption, which show that positive correlations exist between micropores, transition pores, porosity and the coal rank [19]. And the structural stress also had a significant impact on porosity and connectivity of pores as confirmed by atomic force microscopy [20]. However, a few studies have focused on the relationship between coal facies and pore-fracture characteristics, which refer to the primary genetic types, organic petrology, sedimentology, organic geochemistry [21-23].

In this work, firstly, the pore-fracture structure characteristics were investigated with MIP, optic microscopy to coal samples from Sanjiang-Mulinghe coal-bearing basins. Then three coal facies were identified using Q-cluster analysis, TPI-GI, WI -GWI diagram, and the relationship between pores, fractures of coal and coal facies were established. Finally, a new approach predicting favorable areas of CBM reservoir from the perspective of coal facies was proposed.

2. Experiments and methods

2.1. Geological background, sampling and coal analyses

Sanjiang-Mulinghe coal-bearing basins are located in Norheast China, which contain Boli basin, Suibin sag, Hegang basin, Jixi basin and Hulin coal-bearing Basin with abundant CBM resources. Sanjiang-Mulinghe coal-bearing basins have experienced multi-stage tectonics including the middle and late stages of Yanshanian and Himalayan movements in the

Peer-reviewed version available at Energies 2020, 13, 1196; doi:10.3390/en13051196

evolution of the coal-bearing basins, N-S direction Jiaying Fault to the west, the S-N direction Dahezhen Fault to the east, and the N-E direction Dunmi Fault to the southeast are main faults of Sanjiang-Mulinghe coal-bearing basins as shown in Figure 1 [24]. Chengzihe and Qihulin-Yunshan Formations are main coal-bearing strata in this area and formed at the same stage with more than 100 coal seams, thickness of coal lines range between 0.6-2.0 m. The Chengzihe Formation is mainly composed tufa, mudstone, sandstone, and coal seams, in which coal seam about 70 coal seams are available with minable thicknesses less than 29.5 m. The peat mires of these coal-bearing strata developed mainly in the lagoon-gulf and delta plain [8].

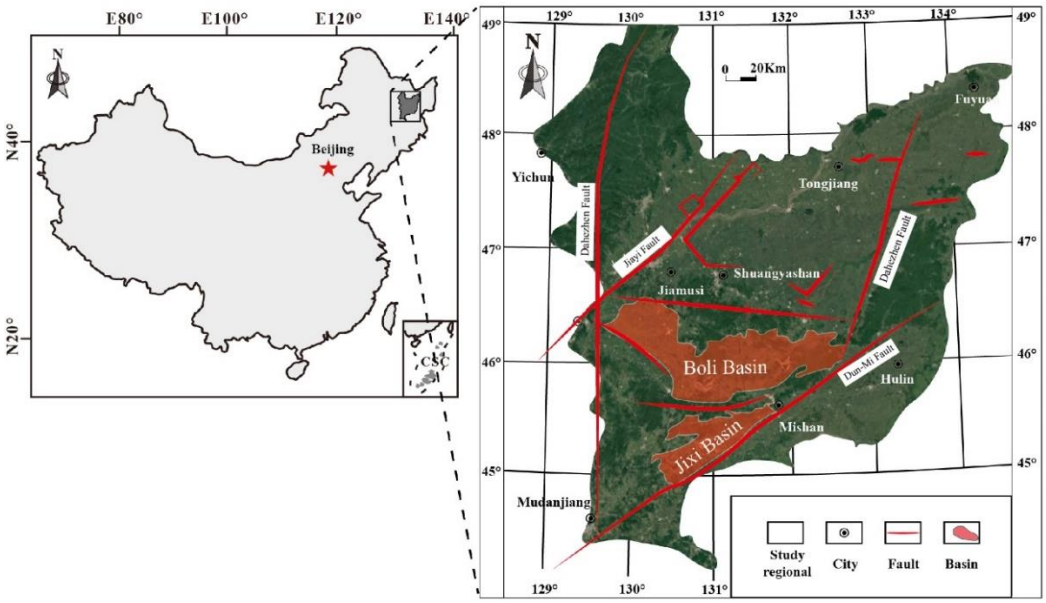

Figure 1. Sampling location of Sanjiang-Mulinghe coal-bearing basins, Northeast China

A total of 38 coal samples were collected from the working faces of Jixi and Boli basin (Figure 1) for coal lithotype analysis, mercury porosimetry, counting microfractures with photometer microscopy. Maximum vitrinite reflectance (Ro, max) and maceral analyses was carried out on polished slabs of approximately 30 × 30 mm^2 in reflected optical light with a Leitz MPV-3 photometer microscope, following China standard GB/T 6948-2008 and GB/T 8899-1998, respectively [25, 26]. Almost these samples are medium volatile bituminous ranks. Proximate analyses were also measured to obtain the percentage of moisture content (air-dried basis), ash yield (air-dried basis), hydrogen content (air-dried basis) and fixed carbon (air-dried basis) based on the Chinese National standards GB/T 30732-2014 (Table 1)

Peer-reviewed version available at *Energies* **2020**, *13*, 1196; doi:10.3390/en13051196

Table 1. Proximate analysis and micro-fracture analysis of selected coals from Sanjiang-Mulinghe coal-bearing basins

Sample No.	Ro,m%	Coal composition				Proximate analysis				Micro-fractures (per 9cm²)				
		V	I	E	M	C,ad	H,ad	M,ad	A,ad	A	B	C	D	Total
NE1	0.49	77.5	8.5	13.6	0.4	70.94	4.87	2.06	10.85	0	0	3	16	19
NE7	0.61	78.3	10.3	11.1	0.3	74.88	7.76	1.48	9.81	2	2	18	52	74
NE10	0.77	76.8	17.5	4.8	0.9	71.6	4.5	1.43	13.42	0	1	29	119	149
NE6	0.8	73.7	19.6	6.2	0.5	82.21	4.86	0.86	4.41	0	2	19	32	53
NE11	0.81	75.9	5.6	18.2	0.3	76.28	5.05	1.02	10.14	0	2	26	63	91
NE26	0.83	93.6	4.8	1.2	0.4	65.1	4.01	1.18	22.03	*	*	*	*	*
NE18	0.87	89.2	1.3	7.5	2	57.48	3.88	1.16	30.67	0	1	29	21	51
NE19	0.9	34	62.7	1.7	1.6	71.5	4.04	0.72	18	0	3	24	213	240
NE14	0.95	79.7	19.1	0.7	0.5	67.5	3.75	0.92	21.81	0	0	6	67	73
NE13	1.05	77.1	15.9	7	0	75.78	4.4	0.77	12.72	0	2	15	51	68
NE12	1.14	81.5	16.1	1.5	0.9	74.27	4. 0	0.9	15. 3	0	0	14	25	39
NE5	1.4	94.7	2	0	3.3	64.58	3.48	0.65	27.54	0	0	15	35	50
NE3	1.6	90.5	6.4	0	3.1	85.14	3.42	0.18	7.54	0	3	49	312	364

* = No data; Ro,m = mean maximum vitrinite reflectance under oil immersion. V = vitrinite; I = inertinite; E = exinite; M= minerals; C, ad =carbon (air-dried basis); H, ad = hydrogen (air-dried basis); M, ad = moisture (air-dried basis); A, ad = ash (air-dried basis); Type of microfractures includes A (W)≥ 5 μm and L ≥ 10 mm), B (W ≥ 5 μm and L ≤ 10 mm), C (W < 5 μm and L ≥ 300 μm) and D (W < 5 μm and L < 300 μm).

Peer-reviewed version available at Energies 2020, 13, 1196; doi:10.3390/en13051196

2.3. Mercury intrusion porosimetry

Mercury intrusion porosimetry (MIP) experiment is the most commonly used method for analyzing the pore characteristics of the porous medium, including porosity, pore structure, pore connectivity and pore compression coefficient. Compared with the gas adsorption method, a more comprehensive range of pore sizes could be measured with MIP, including pore characteristics of mesopore and macropore that cannot be measured by the gas adsorption method. During the MIP experiment, the higher the pressure of mercury injection, the smaller the measured pore size.

Washburn equation [27], can be adopted to obtain pore radius, as follows:

$$r_{max} = -\frac{2\sigma cos\theta}{P_T} \quad (1)$$

Where P_T is mercury injection pressure, MPa; σ is surface tension, set to be 0.48 J/m^2; θ is the contact angle between mercury and coal, set to be 141°; r_{max} is the maximum capillary radius, μm. Thus, the equation could be substituted:

$$r_{max} = \frac{0.746}{P_T} \quad (2)$$

2.4. Microfractures statistics by optical microscope

The microfractures of coal refer to fracture with the width at the micron scale, which links pores and cleats of coal and plays a crucial role in CBM extraction [28]. The microfractures of coal were counted by LABORLXE 12 POL optical microscope and coal samples processing procedures are the same as presented in our previous work [29]. The microfractures could be divided into four types based on their width (W) and length (L) in this work [30]: type A (W ≥ 5 μm and L ≥ 10 mm), type B (W ≥ 5 μm and L ≤ 10 mm), type C (W < 5 μm and L ≥ 300 μm) and type D (W < 5 μm and L < 300 μm).

The microfracture frequency of coal could be determined quantitatively with the optical microscope, which is defined as the total microfracture number within 9 cm^2 (fracture frequency with per 9 cm^2). The microfractures morphologies involving dendritic, filamentous, orthogonal and X-shaped, and connectivity of also can be acquired.

2.5. Coal facies identification

Coal petrology characteristics are an essential sign of paleo-environmental conditions, maceral composition and content depend on the plant species and their composition of the swamp water to a large extent. Previous research have developed four coal maceral indexes, including tissue preservation index (TPI), gelification index (GI), wood index (WI), groundwater index (GWI), to reveal information on coal-forming plants, swamp water condition, and sedimentary environment during coalification and classify coal facies [19, 31].

TPI is the percentage of tissue degradation on wood in coal-forming plants, reflecting the intensity of microbiological deterioration and demonstrating the PH value in the environment. Generally, a low PH-value environment corresponds to a high TPI value, which can better preserve the plant tissues because the weaker microbial activity leads to weak biochemical degradation in this environment. Meanwhile, the TPI is also an essential parameter of the proportion of woody plants in the paleo-environmental.GI represents the ratio between gelation components and nongelation components reflecting water table in the peat mire and the degree of gelification. The higher GI, the greater the gelification and the

Peer-reviewed version available at Energies 2020, 13, 1196; doi:10.3390/en13051196

wetter the peat mire. WI was first proposed to characterize as coal-forming vegetation and the degree of plant preservation[32]. The GWI implies the intensity of rheotropic conditions as a ratio of the gelification and mineral matter contents in coal during the period of peat accumulation. A higher GWI value indicates a higher mineral content and higher water levels, which means that peat mire is rheotropic. A combined classification from pervious scholars for coal facies is used in this study [19,31]: dry forest swamp (0<GI <1 and TPI>1), wet forest swamp (GI>1 and TPI >1), rheotropic environment (GWI>1), mesotrophic environment (0.5<GWI<1), ombrotrophic environment (GWI>1).

The four facies indexes could be calculated by the following formulas [19]:

$$TPI = \frac{Telinite + Collotelinite + Semifusinite + Fusinite}{Collodetrinite + Macrinite + Inertodetrinite} \quad (3)$$

$$GI = \frac{Vitrinite + Macrinite}{Semifusinite + Fusinite + Inertodetrinite} \quad (4)$$

$$WI = \frac{Telinite + Collotelinite}{Collodetrinite + Vitrodetrinite} \quad (5)$$

$$GWI = \frac{Gelinite + Corpogelinite + Minerals + Vitrodetrinite}{Telinite + Collotelinite + Collodetrinite} \quad (6)$$

3. Results and discussion

3.1. Pore characteristics

In the MIP experiment, different mercury intrusion and extrusion curves illustrate the connectivity, pore size, and distribution of coal reservoirs [33]. Pores characteristics of various coal samples with MIP are presented in Table 2. The porosity and the total pore volume are 1-7% and 8.23 - 11.7 cm^3, respectively. Pore-throat diameters vary from 0.03 μm - 0.36 μm and the corresponding average pore-throat diameter is 0.116 μm. Figure 2 presents the significant heterogeneity in pore size distribution (PSD), the proportion of micropores and transition pores (<100 nm) for most coal samples are higher than mesopore and super pores/microfractures except sample NE12 and sample NE38. The average percentage of pores with diameters less than 100 nm is 68.25%, the pores with diameters larger than 100 nm account for 31.75%.

Peer-reviewed version available at Energies 2020, 13, 1196; doi:10.3390/en13051196

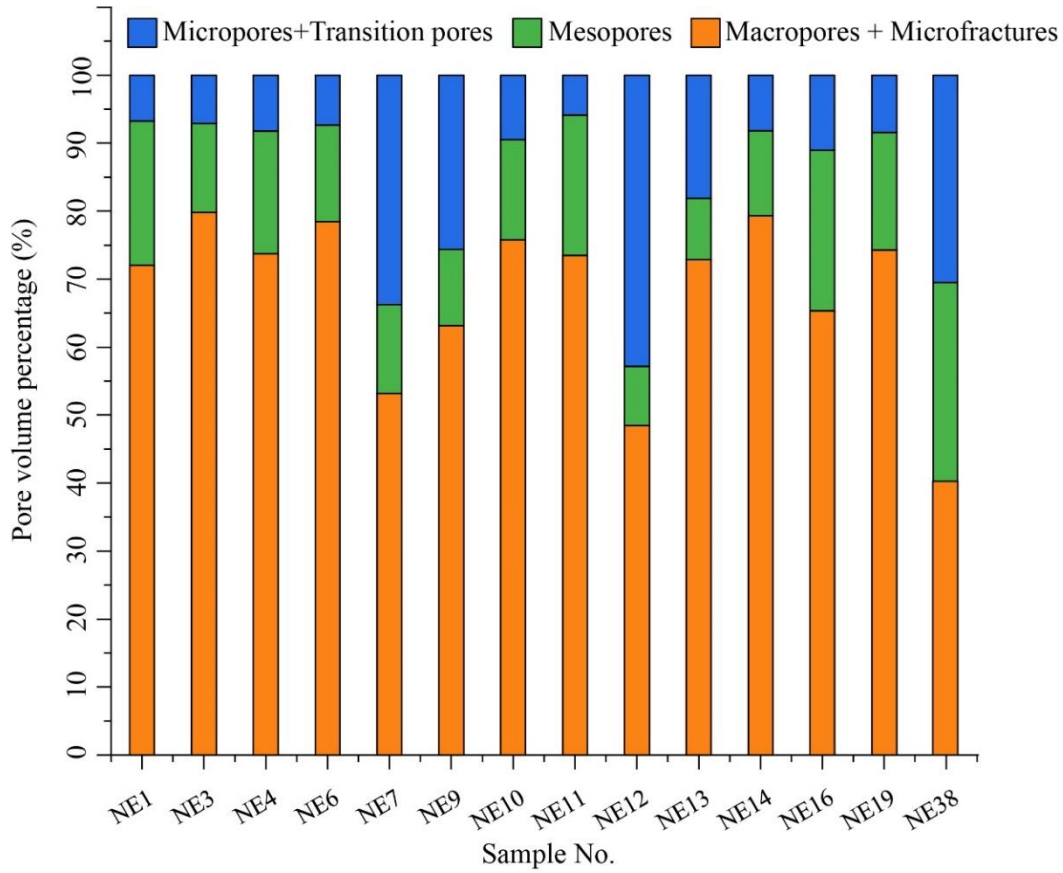

Figure 2. The pore volume distribution of selected coals from Sanjiang-Mulinghe coal-bearing basins

Three types of mercury injection curves were classified of 14 coal samples as shown in Table 2. Type Ⅰ is represented by sample NE14 as shown in Figure 3a, the mercury injection curve is divided into two distinct stages, including rapid rise stage and smooth curve stage, the rapid rise stage in low-pressure condition indicates that with the increment of pressure, mercury is difficult inject into pore of coal, when pressure increase from 0 MPa to 1 MPa, the mercury volume saturation shows less change with rising from 0 to 20% after the pressure greater than 1 MPa, the mercury injection is relatively stable and the injection curve is relatively smooth. This type of mercury injection curve has high mercury saturation and high efficiency of mercury withdrawal with 80% and 81.25% respectively, which indicates micropores and transition pores are dominated based on Equation (1), meanwhile, the pores are well connected due to the high efficiency of mercury withdrawal. Type Ⅱ is represented by sample NE9 with three stages—straight-line stage, rapid rise stage and smooth curve stage as shown in Figure 3b; for this type, the proportion of adsorption-pores which calculated by MIP are nearly 63.12%, and macropores and microfractures are better developed than type Ⅰ. Obviously, mercury injection curve for type Ⅲ has four stages, including rapid rise stage, platform stage, rapid rise stage and smooth curve stage. Additionally, mercury intrusion saturation over 90% and the extrusion of mercury saturation is relatively low, only 32.1%, which indicates the pores are not well connected. There are two rapid rise stages so that micropores and transition pores are not well developed, at only 40.42% and two peaks of pore size distribution could be found in Figure 3c.

Peer-reviewed version available at *Energies* **2020**, *13*, 1196; doi:10.3390/en13051196

Table 2. Pore analysis and mercury porosimetry results of the selected coal samples

Smaple No.	Porosity (%)	IMS (%)	EMS (%)	PTM (μm)	Total volume (cm^3)	Pore volume distribution (%)			Type of IMC
						V1	V2	V3	
NE 1	1.8	64.9	26.869	0.12	10.26	72.07	21.2	6.73	I
NE 3	1	68.82	16.41	0.06	10.69	79.8	13.12	7.08	I
NE 4	1	70.69	18.16	0.1	11.7	73.72	18.02	8.27	I
NE 6	1.4	69.31	14.55	0.1	8.23	78.48	14.15	7.37	I
NE 7	1.7	84.02	39.23	0.07	9.58	53.21	13.03	33.76	III
NE 9	4.9	60.89	39.95	0.07	10.53	63.12	11.2	25.68	II
NE 10	3.3	52.23	25.13	0.17	10.66	75.81	14.72	9.47	I
NE 11	1.9	70.83	19.32	0.12	8.06	73.49	20.66	5.85	I
NE 12	3.2	83.02	55.38	0.03	11	48.44	8.75	42.81	III
NE 13	2.7	56.93	28.94	0.04	9.62	72.86	9.02	18.12	III
NE 14	1.5	63.65	16.01	0.06	10.29	79.31	12.53	8.16	I
NE 16	4.2	66.38	40.31	0.36	10.64	65.32	23.64	11.05	II
NE 19	1.8	34.99	20.87	0.11	10.57	74.28	17.32	8.4	I
NE 38	3.3	91.86	62.37	0.16	10.23	40.24	29.26	30.46	III

IMS = Injection of mercury saturation (%); EMS = Extrusion of mercury saturation (%); PTM=Pore throat mean (μm); IMC = Injection of mercury curves; V1= Pore diameter smaller than 100 nm; V2 = Pore diameter ranges from 10^2 to 10^3 nm; V3= Pore diameter ranges larger than 10^3 nm.

Peer-reviewed version available at Energies 2020, 13, 1196; doi:10.3390/en13051196

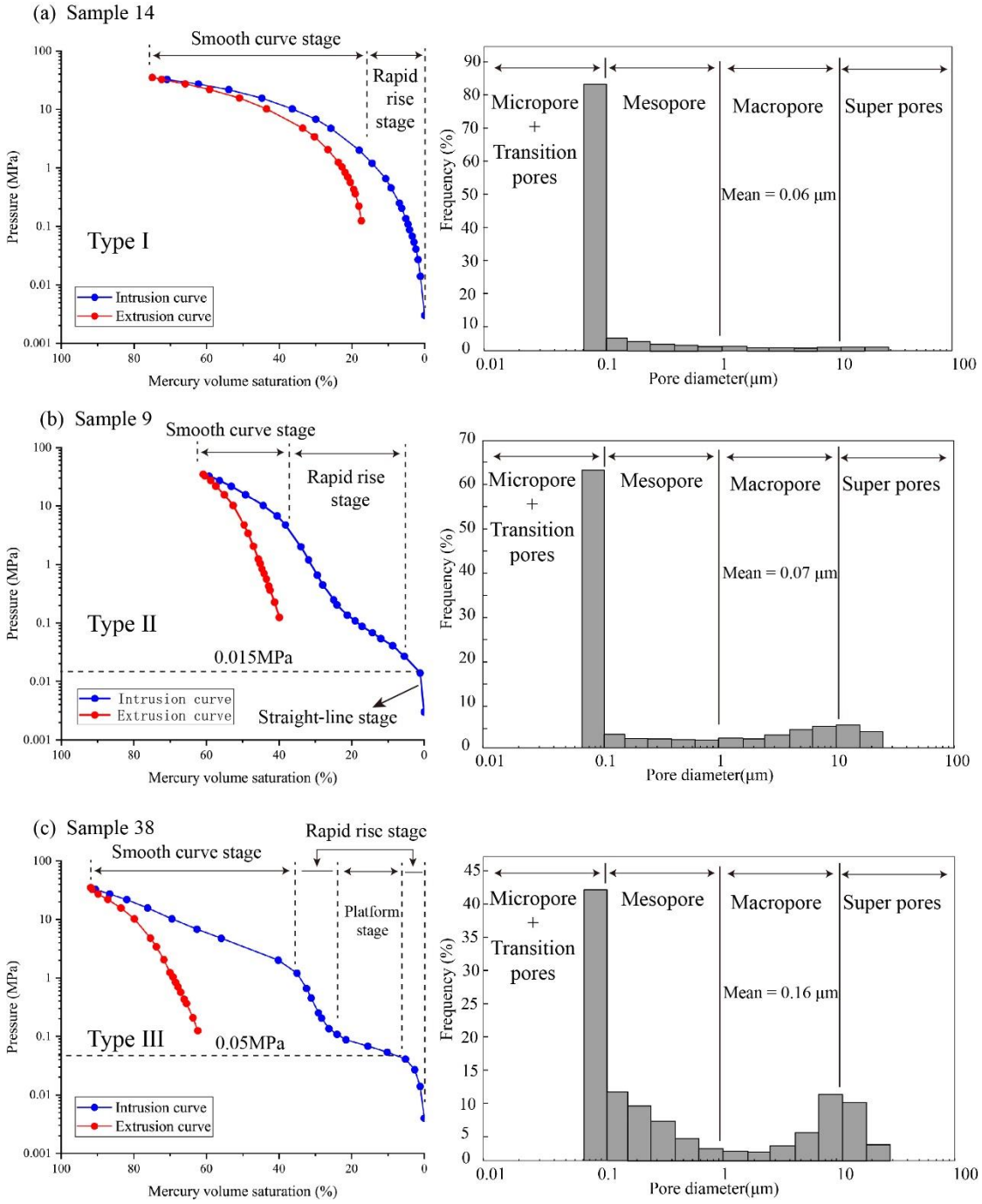

Figure 3. The pore size and volume distribution of 15 coal samples from Sanjiang-Mulinghe coal-bearing basins

3.2. Microfracture characteristics

The microfractures frequency and morphology characteristics of different coal samples are shown in Figure 4 and Table 1. Type D microfractures, are most abundant and display the best-developed with account for more than 70% of the total microfractures in the Sanjiang-Mulinghe coal-bearing basins, which has a wide gap of density ranging from 12 to 312 per 9 cm^2 with an average number of 58.1 per cm^2, filamentous, orthogonal and X-shaped and are the dominant morphology for type D microfracture (Figure 4.). Type C microfractures are secondly developed with range from 3 to 60 per 9 cm^2, with an average number of 19.8 per 9 cm^2, while type A and B microfractures are poorly developed with account for less than 2 per

Peer-reviewed version available at Energies 2020, 13, 1196; doi:10.3390/en13051196

9 cm², moreover, some coal samples without developed this kind of fracture (such as sample NE5, NE6, NE7), which indicates it is different for CBM to migrate from pores to microfractures and cleats.

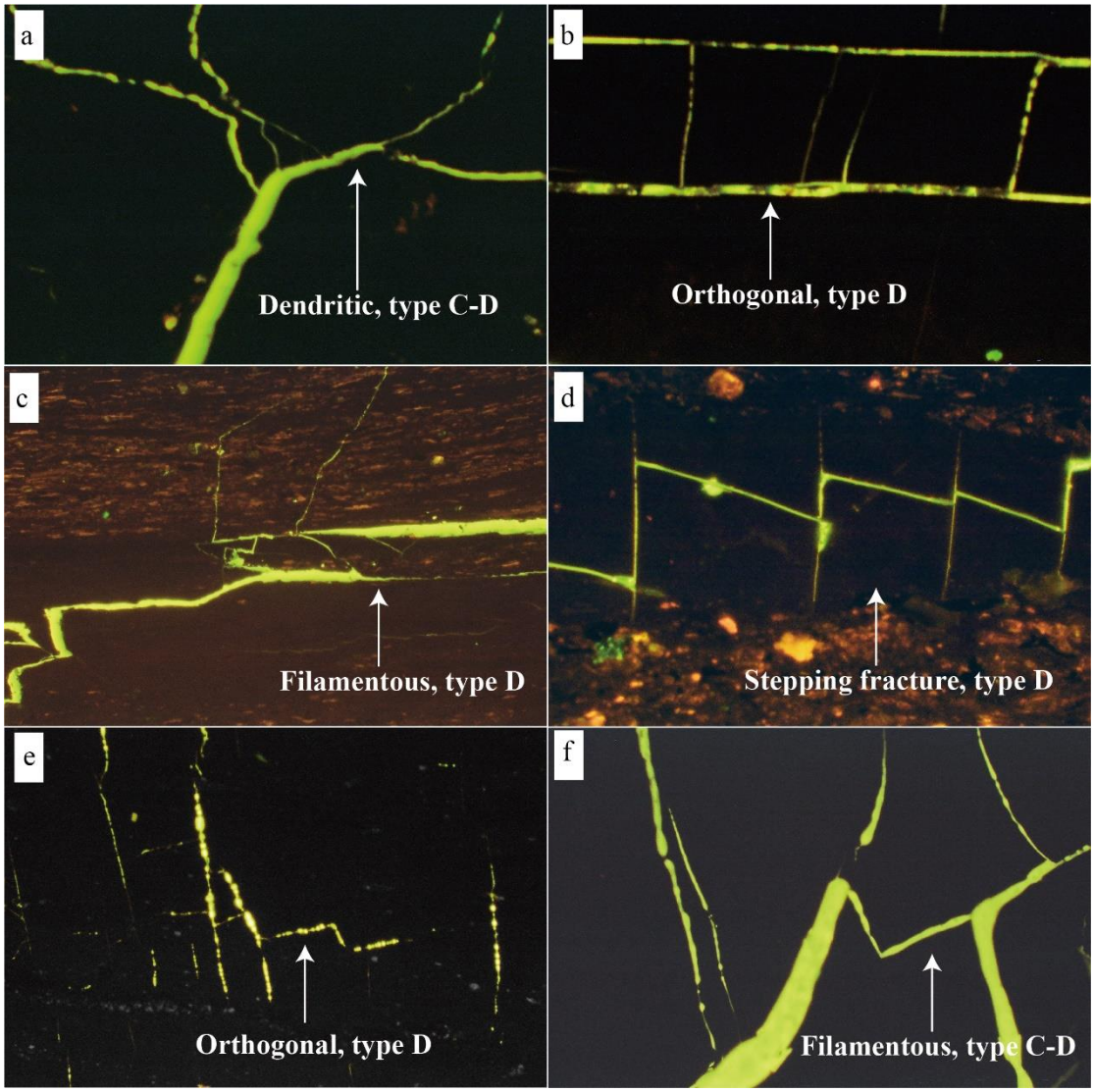

Figure 4. Morphology and frequency of endogenous microfractures observed by optical microscope (×63). (a)Sample NE19, Dendritic, F=213;(b) Sample NE14, orthogonal, F=67; (c)Sample NE22, filamentous, F=25;(d) Sample NE4, orthogonal, F=30;(c) Sample NE25, orthogonal, F=137;(d) Sample NE31, filamentous, F= 61

3.3. Effects of coal facies on pore-fracture performance

3.3.1. Characteristics of coal facies

The results of TPI, GI, WI, and GWI are calculated in Table 3 from the formula in section 2.5, as shown in Table 3, the TPI and GI value in this block is generally more massive than the previous with TPI range from 0.3 to 47 and GI range from 1 to 106, which indicates that woody plants are dominated and plants with high in preservation potential at the paleo-environmental. Almost all of the samples are located in the wet forest swamp region with pervious methods in section 2.5. For more detail of coal facies, Q-cluster analysis (farthest neighbor), and GI-TPI and WI-GWI plate were applied, Q-cluster analysis is a multivariate statistical analysis method that classifies the objects with the similar relationship of the

Peer-reviewed version available at Energies 2020, 13, 1196; doi:10.3390/en13051196

research object. It can classify similar samples based on the observation parameters (TPI, GI, WI, GWI in this work) of the samples and the degree of similarity between specific calculated samples [34]. Three various coal facies (coal facies 1, coal facies 2 and coal facies 3) were distinguished by Q-cluster analysis as shown in Figure 5.

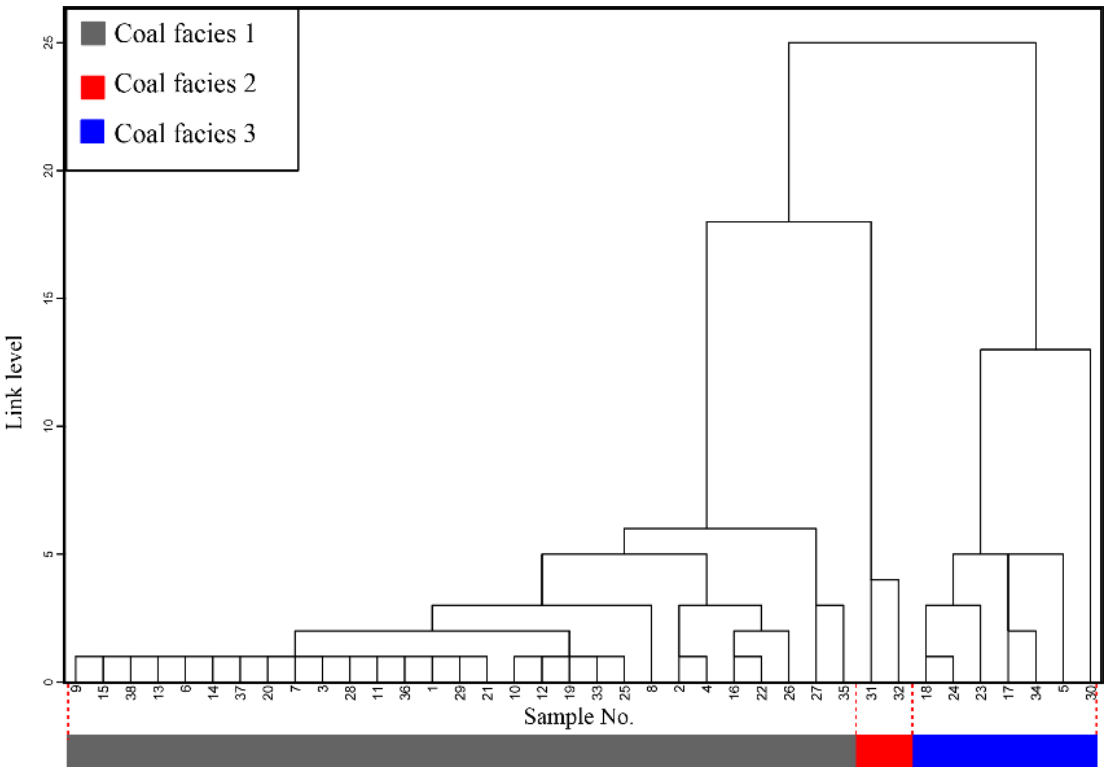

Figure 5. Dendrogram showing coal facies results of Q-cluster analysis

Combined with the distribution characteristics of coal samples in the GI-TPI diagram (Figure 6.), the Q-clustering results could be adjusted appropriately on the basis of the Q-cluster method. The ash content of sample NE26 is significantly higher than other samples in coal facies 1(Table 1), which reflect severe water dynamic condition and low water table, thus sample NE26 was reclassified into the coal facies 3.Three types of coal facies could be denominated as Type Ⅰ, Type Ⅱ, and Type Ⅲ, (Table 3, Figure 6) finally. Three types of coal facies are the upper delta plain wet forest swamp, lake shore coastal wet forest swamp, tidal flat wet forest swamp, respectively.

Lakeshore coastal wet forest swamp is characterized by high water level and good tissue preservation, the dominant source for the peat is herbaceous arborescent assembly of plants in peat formation, this facies has low TPI (1<TPI<15), low GI (1<GI<25), low WI (1<WI<15) and low GWI (<0.1). The upper delta plain wet forest swamp is dominated by woody plants with the high water table and good tissue preservation, high TPI (>15), low GI (1<GI<25), high WI (>40), low GWI (<0.1).The characteristics of tidal flat wet forest swamp are low water table and high gelification, in such condition, semi-bright coal and bright coal are the main lithotypes and the ash content of coal is high with more than 20% due to the tidal action, this facies has high TPI (>15), high GI (>25), high WI (>40), and low GWI (<0.1).

Peer-reviewed version available at Energies 2020, 13, 1196; doi:10.3390/en13051196

Table 3. Coal facies indexes and coal facies type in Sanjiang-Mulinghe coal-bearing basins

Sample No.	Coal face indexes				Coal facies types	Sample No.	Coal face indexes				Coal facies types
	TPI	GI	WI	GWI			TPI	GI	WI	GWI	
NE1	9.9	9.1	13	0.01	Type Ⅰ	NE 20	5	13	5	0.04	Type Ⅰ
NE2	19.1	25.7	38	0.01	Type Ⅲ	NE 21	12	7	14	0.02	Type Ⅰ
NE3	13.1	14.1	8.8	0.08	Type Ⅰ	NE 22	12	7	22	0.04	Type Ⅰ
NE4	12.9	15.8	36	0.03	Type Ⅰ	NE 23	15	83	16	0.06	Type Ⅲ
NE5	26.2	47.4	25	0.05	Type Ⅲ	NE 24	23	68	27	0.03	Type Ⅲ
NE6	7.8	4.3	10	0.05	Type Ⅰ	NE 25	5	9	7	0.03	Type Ⅰ
NE7	0.3	7.6	0.2	0.04	Type Ⅰ	NE 26	33	20	26	0.03	Type Ⅲ
NE 8	3.9	24.7	4.2	0.14	Type Ⅰ	NE 27	12	20	16	0.01	Type Ⅰ
NE 9	5.3	7	6.4	0.01	Type Ⅰ	NE 28	9	17	11	0.04	Type Ⅰ
NE 10	6	4	9	0.04	Type Ⅰ	NE 29	11	9	17	0.03	Type Ⅰ
NE 11	14	14	14	0	Type Ⅰ	NE 30	27	106	30	0.01	Type Ⅲ
NE 12	4	5	7	0.03	Type Ⅰ	NE 31	47	22	56	0.04	Type Ⅱ
NE 13	4	5	4	0.02	Type Ⅰ	NE 32	18	9	58	0.09	Type Ⅱ
NE 14	5	4	9	0.02	Type Ⅰ	NE 33	2	2	3	0.04	Type Ⅰ
NE 15	6	7	7	0.03	Type Ⅰ	NE 34	35	52	18	0.04	Type Ⅲ
NE 16	7	4	28	0.05	Type Ⅰ	NE 35	2	3	3	0.14	Type Ⅰ
NE 17	19	60	5	0.26	Type Ⅲ	NE 36	8	10	15	0.09	Type Ⅰ
NE 18	22	69	33	0.02	Type Ⅲ	NE 37	3	6	3	0.01	Type Ⅰ
NE 19	7	1	9	0.05	Type Ⅰ	NE 38	6	7	7	0.07	Type Ⅰ

TPI= Tissue preservation index; GI= Gelification index; WI= Wood index; GWI= Groundwater influence index

Peer-reviewed version available at Energies 2020, 13, 1196; doi:10.3390/en13051196

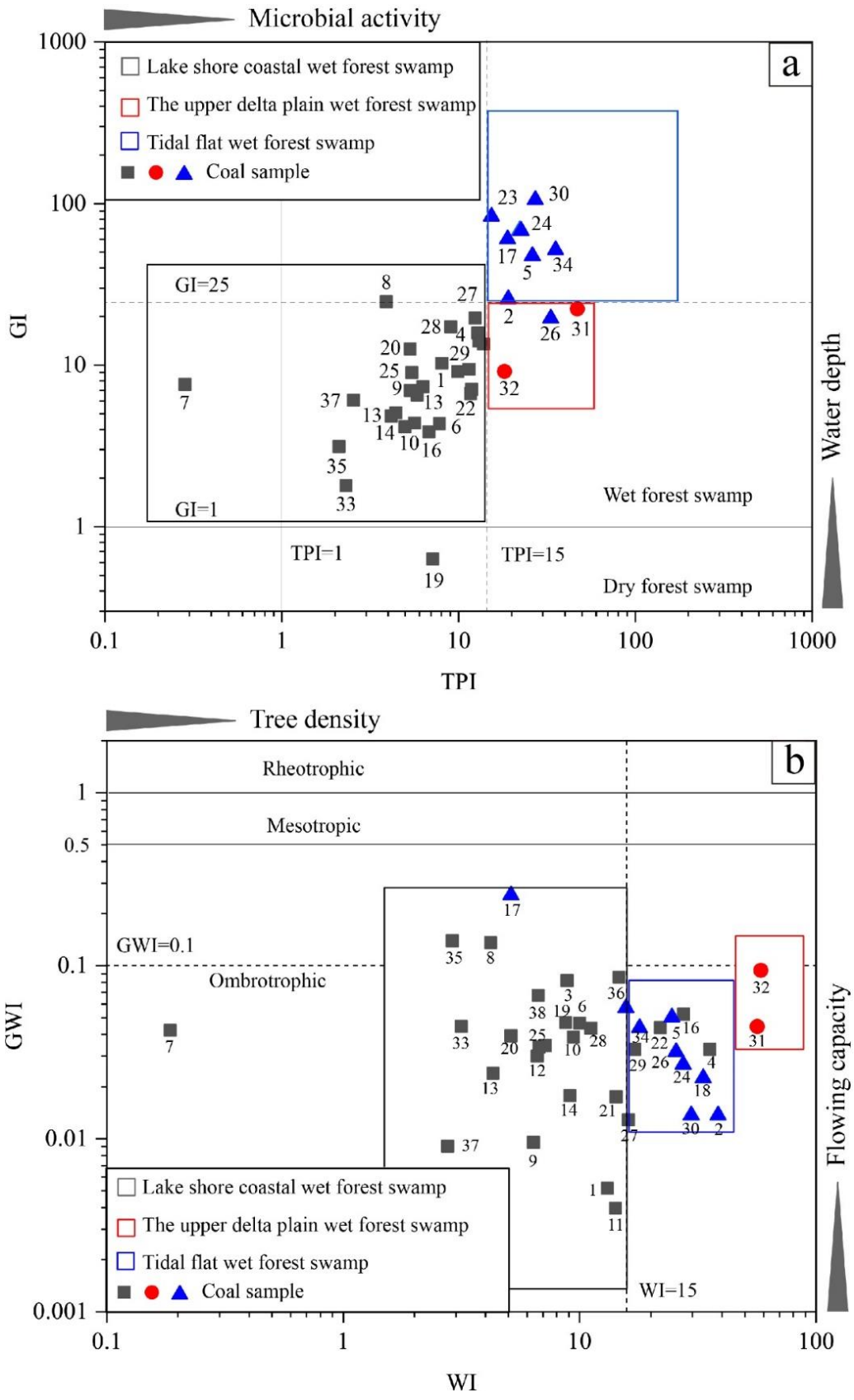

Figure 6. Coal facies interpretation from Sanjiang-Mulinghe coal-bearing basins. (a) GI - TPI, (b) GWI – WI

Peer-reviewed version available at Energies 2020, 13, 1196; doi:10.3390/en13051196

3.3.2. Effects of coal facies on pore development

The paleo-environmental governs the degree of pore development by affecting the petrographic composition and content of macerals [35]. Zhang et al. studies have found that the macro- and mesopores are closely correlated to TPI with the R-cluster analysis method, while there is no data to support the specific relationship between pore and coal facies[20]. As shown in Figure 7a2, Figure 7a3, Figure 7c2, Figure 7c3, there is obvious relationship between coal facies and pore development, as the value of TPI and WI increased, the percentage of micropores and transition pores (<10^2nm) increases and negative correlation between TPI or WI and macropores could be observed, while there is no significant correlation between pore size which between 10^2 nm and 10^3 and coal facies index. The origin of macropore, beginning with the space in residual cell structures of precursor plants or among mineral particles, high TPI meaning rapid peat accumulation process with short effective time of gelification, plant cell structures are well preserved, and poorly developed macropores of coal, thus, the proportion of macropores of coal is highly correlated to the TPI, and TPI could indicate the seepage characteristics of coal.

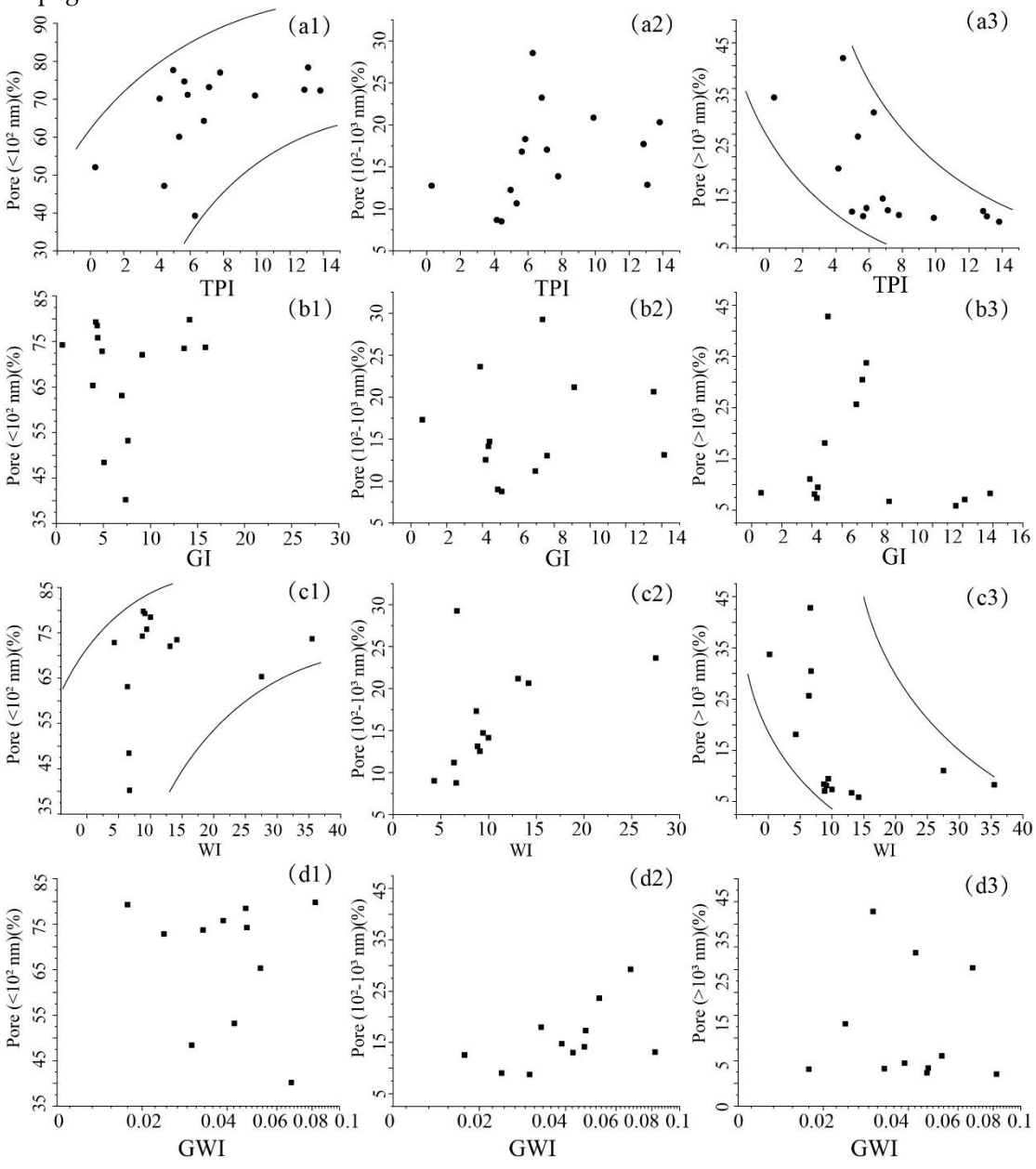

Figure 7. Relationships between the pore size and coal facies index (TPI, GI, WI, GWI)

Peer-reviewed version available at Energies 2020, 13, 1196; doi:10.3390/en13051196

3.3.3. The effects of coal facies on fracture

Figure 8 shows the correlation analysis between coal facies index (GWI) and various types (Type A, B, C and D) fractures for all coal samples. For type A and type B fractures, which are slightly developed in the coal samples with a range from 0 to 2 and 0 to 3 per 9 cm^2 respectively and these two kinds of types fractures do not have any trend with the GWI. Fracture frequency of Type C and Type D shows a positive relationship as GWI increase, as shown in Figure 8c, Figure 8d. The GWI reflect flowing capacity as shown in Figure 6b, the high value of GWI indicates unstable conditions and high groundwater table during the period of peat accumulation, meanwhile, high GWI indicates high amounts of minerals based on the formula in section 2.5. Generally, organic matter is more hydrophobic than clay minerals and other mineral grains [35], hydration has significant impact on fracture developed in coal reservoir, since mineral would be swelling in reaction to water-based fluid, primary fracture would expand in with and length, and would create new fractures in hydration, which makes pore-fractures network more completed and has good connectivity between pores and fractures [36]. Based on the relationship between GWI and different kinds of fractures and the effects of hydration on fractures, we can find the hydration of mineral has no effect on type A and type B fractures and great effect on type A and type B fractures developed in coal.

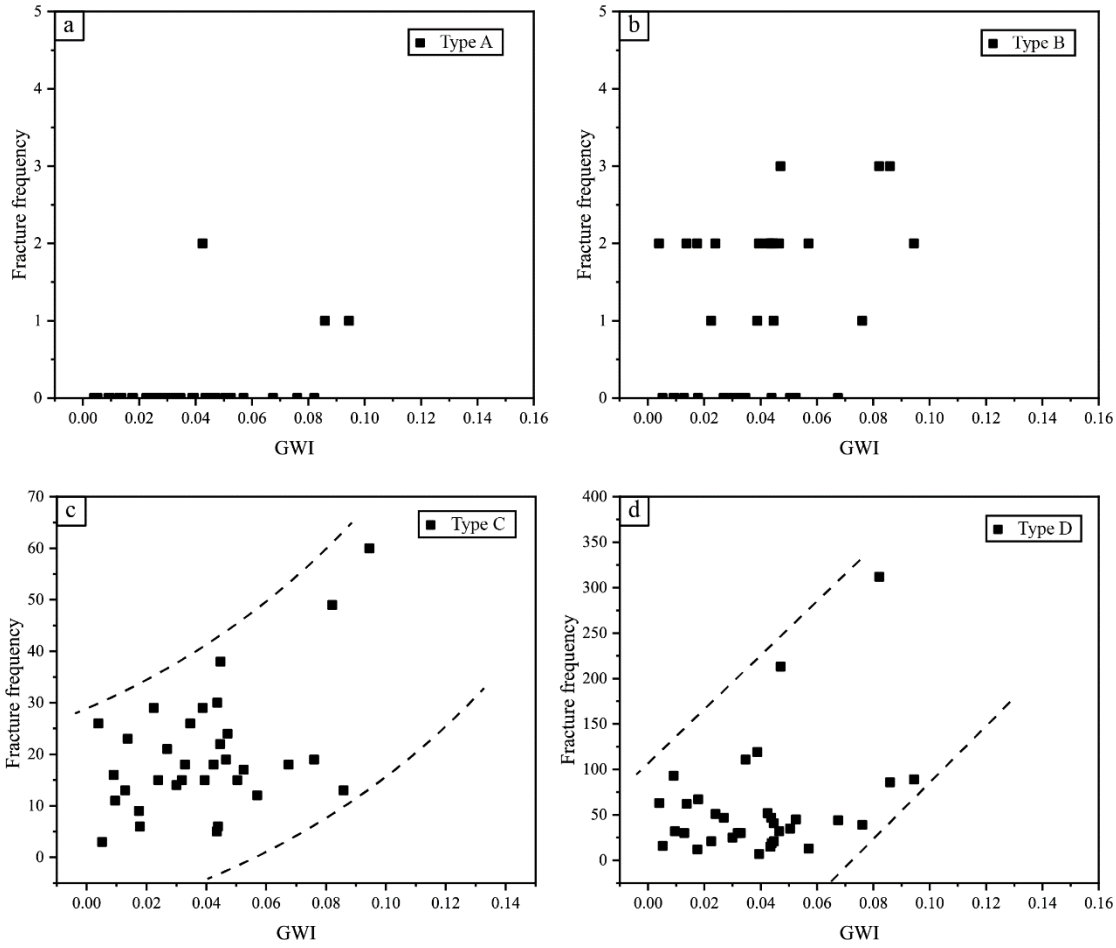

Figure 8. Relationships between the microfractures and coal facies index (GWI). (a)GWI against type A fractures; (b) GWI against type B fractures; (c) GWI against type C fractures; (d) GWI against type D fractures

3.4. Prediction of CBM reservoir favorable areas with coal facies

Peer-reviewed version available at Energies 2020, 13, 1196; doi:10.3390/en13051196

Adsorption capacity and diffusion/seepage capacity are two key indicators for CBM reservoir, which would affect the CBM enrichment and production directly [37]. On the above basis, the percentage of micropores and transition pores related to the TPI and WI, the frequency of type C and type D increases as GWI is increased. Thus, we consider there is another function for WI-GWI diagram- favorable areas evaluation in CBM reservoir. The WI-GWI diagram could be divided into four areas, including 'strong adsorption, well connectivity' area, 'weak adsorption, well connectivity' area, 'weak adsorption, poor connectivity' area, and 'strong adsorption, poor connectivity' area as shown in Figure 9. By combining the results of coal facies identification in Section 3.3.1, we found the coal facies of upper delta plain wet forest swamp is the most favorable area for CBM production with strong adsorption and well connectivity of coal reservoir and Lake shore coastal wet forest swamp is not benefit for CBM enrichment and gas migration in the coal reservoir.

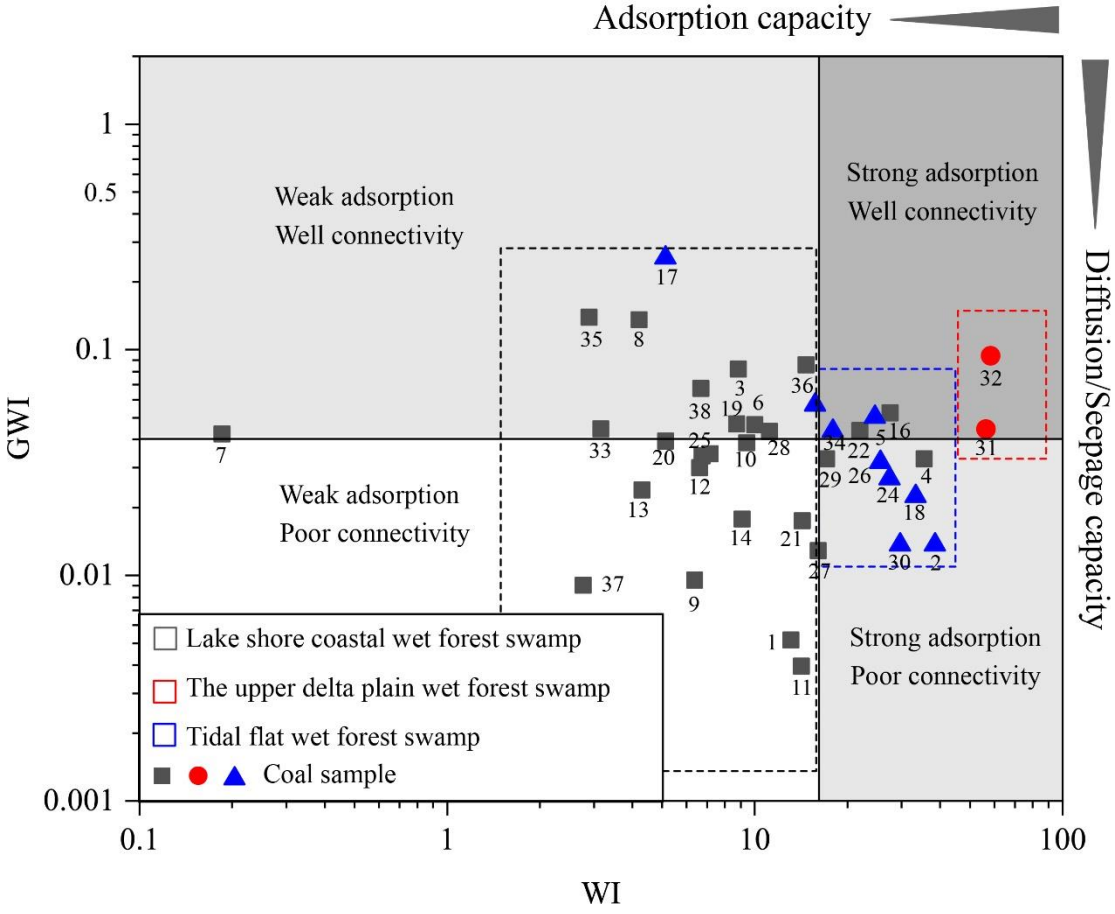

Figure 9. Favorable areas evaluation of CBM reservoir with GWI-WI diagram

4. Conclusions

The pore-fracture structure and coal facies of different coal samples from the Sanjiang-Mulinghe coal-bearing basins were investigated by MIP, optical microscope, and Q-cluster analysis. The following conclusions can be made:

1) Micropores and transition (<100 nm) pores are most abundant and display the best-developed for all coal samples with an average percentage is 68.25%. Three types of mercury injection curve were classified based on MIP experiment, and type Ⅱ is good for CBM flow in the coal reservoir due to the high porosity of macropores and well connectivity of pores in coal reservoir.

2) Type D microfractures are most abundant and display the best-developed microfractures with account for more than 70% of the total microfractures. The hydration of

Peer-reviewed version available at Energies 2020, 13, 1196; doi:10.3390/en13051196

mineral has little effect on type A and type B fractures, whereas it has great effect on type C and type D fractures developed in coal.

3) Three types of coal facies were identified based on the Q-cluster analysis, GI-TPI and GWI-WI diagrams, including lake shore coastal wet forest swamp, the upper delta plain wet forest swamp, tidal flat wet forest swamp, respectively. There is positive correction between TPI, WI and micropores, a negative correlation between TPI, WI and macropores/fractures.

4) The WI-GWI diagram also could be used to evaluate favorable areas in CBM reservoir based on the effects of WI, GWI on pore and fractures characteristics. The upper delta plain wet forest swamp is optimization of favorable areas of CBM reservoir with strong adsorption and well connectivity of pores for Sanjiang-Mulinghe coal-bearing basins.

Author Contributions: Dameng Liu and Yidong Cai conceived and designed the experiments; Yuejian Lu performed the experiments and wrote the paper; Yuejian Lu and Yidong Cai analyzed the data; Dameng Liu and Yidong Cai revised the paper and provided language support; Qian Li, Qifeng Jia provided technical support.

Acknowledgments: This research was funded by the National Natural Science Fund (grant nos. 41830427, 41772160 and 41922016) and the Fundamental Research Funds for Central Universities (grant no. 2652018002).

Conflicts of Interest: The authors declare no conflict of interest.

References

1. Yao, Y.B.; Liu, D.M.; Liu, J.G.; Xie, S.B. Assessing the Water Migration and Permeability of Large Intact Bituminous and Anthracite Coals Using NMR Relaxation Spectrometry. Transport. Porous. Med. 2015, 107, 527-542.
2. Scott, A.R. Hydrogeologic factors affecting gas content distribution in coal beds. Int. J. Coal Geol. 2002, 50, 1-4, 363–387.
3. Wang, B.; Sun, F.J.; Tang, D.Z.; Zhao, Y.; Song, Z.H.; Tao, Y. Hydrological control rule on coalbed methane enrichment and high yield in FZ Block of Qinshui Basin. Fuel, 2015, 140, 15, 68–577.
4. Li, Z.T.; Liu, D.M..; Cai, Y.D.; Ranjith, P.G.; Yao, Y.B. Multi-scale quantitative characterization of 3-D pore-fracture networks in bituminous and anthracite coals using FIB-SEM tomography and X-ray M-CT. Fuel 2017, 209, 1, 43–53.
5. Pashin, J.C. Variable gas saturation in coalbed methane reservoirs of the Black Warrior Basin: Implications for exploration and production. Int. J. Coal Geol. 2010, 82, 3-4, 135–146.
6. Cai, Y.D.; Liu, D.M.; Yao, Y.B; Li, J.Q.; Qiu, Y.K. Geological controls on prediction of coalbed methane of No. 3 coal seam in Southern Qinshui Basin, North China. Int. J. Coal. Geol. 2011, 88, 2-3, 191-104.
7. Zhao, J.L.; Tang, D.Z.; Xu, H.; Lv, Y.M.; Tao, S. High production indexes and the key factors in coalbed methane production: A case in the Hancheng block, southeastern Ordos Basin, China. J. Pet. Sci. Eng. 2015, 130, 55–67.
8. Wang Z.Z; Pan, J.N, Hou, Q.L.; Yu, B.S.; Li, M.; Niu, Q.H. Anisotropic characteristics of low-rank coal fractures in the Fukang mining area, China. Fuel. 2018, 211, 1, 182-193.
9. Ouyang, Z.Q.; Liu, D.M.; Cai, Y.D.; Yao, Y.B. Investigating the fractal characteristics of pore-fractures in bituminous coals and anthracites through fluid flow behavior. Energ. Fuel. . 2016, 30, 12, 10348–10357.
10. Cai, Y.D.; Liu, D.M.; Mathews, J.P.; Pan, Z.J.; Elsworth, D.; Yao, Y.B.; Li, J.Q.; Guo, X.Q. Permeability evolution in fractured coal - Combining triaxial confinement with X-ray computed tomography, acoustic emission and ultrasonic techniques. Int. J. Coal. Geol. 2018, 122, 1, 91-104.
11. Hodot, B.B. Outburst of Coal and Coalbed Gas (Chinese Translation). China Coal Ind. Press. Beijing 1966, 318.
12. Cai, Y.D.; Liu, D.M.; Pan, Z.J.; Yao, Y.B.; Li, J.Q.; Qiu, Y.K. Pore structure and its impact on CH4 adsorption capacity and flow capability of bituminous and subbituminous coals from Northeast China. Fuel. 2013, 103, 258–268.

Peer-reviewed version available at Energies 2020, 13, 1196; doi:10.3390/en13051196

13. Wang, H.C.; Fu, X.H.; Jian, K.; Li, T.; Luo, P.P. Changes in coal pore structure and permeability during N2 injection. J. Nat. Gas Sci. Eng. 2015, 27, 2, 1234–1241.
14. Rodrigues, C.F.; Lemos De Sousa, M.J. The measurement of coal porosity with different gases. Int. J. Coal Geol. 2002, 48, 245–251.
15. Wang, G.; Qin, X.J.; Shen, J.N.; Zhang, Z.Y.; Han, D.Y.; Jiang, C.H. Quantitative analysis of microscopic structure and gas seepage characteristics of low-rank coal based on CT three-dimensional reconstruction of CT images and fractal theory. Fuel. 2019, 256,115900.
16. Chalmers, G.R.L.; Ross, D.J.K.; Bustin, R.M. Geological controls on matrix permeability of Devonian Gas Shales in the Horn River and Liard basins, northeastern British Columbia, Canada. Int. J. Coal Geol. 2012, 103, 120–131.
17. Huang, B.X.; Liu, C.Y.; Fu, J.H; Guan, H. Hydraulic fracturing after water pressure control blasting for increased fracturing. Int. J. Rock Mech. Min. Sci. 2011, 48, 6, 976–983.
18. Cheng, W.; Jin, Y.; Chen, M. Reactivation mechanism of natural fractures by hydraulic fracturing in naturally fractured shale reservoirs. J. Nat. Gas Sci. Eng. 2015, 27, 3, 1357–1365.
19. Wang, F.; Cheng, Y.P.; Lu, S.Q.; Jin, K.; Zhao, W. Influence of coalification on the pore characteristics of middle-high rank coal. Energ. Fuel. 2014, 28, 9, 5729–5736.
20. Pan, J.N.; Zhu, H.T.; Hou, Q.L.; Wang, H.H.; Wang, S. Macromolecular and pore structures of Chinese tectonically deformed coal studied by atomic force microscopy. Fuel, 2015, 139, 1, 94–101.
21. Zhang, S.H.; Tang, S.H.; Tang, D.Z.; Pan, Z.J.; Yang, F. The characteristics of coal reservoir pores and coal facies in Liulin district, Hedong coal field of China. Int. J. Coal Geol. 2010, 81, 2, 117–127.
22. Cecil, C.B.; Stanton, R.W.; Neuzil, S.G.; Dulong, F.T.; Ruppert, L.F.; Pierce, B.S. Paleoclimate controls on late paleozoic sedimentation and peat formation in the central appalachian basin (U.S.A.). Int. J. Coal Geol. 1985, 5, 1-2, 195–230.
23. Mastalerz, M.; Kvale, E.P.; Stankiewicz, B.A.; Portle, K. Organic geochemistry in Pennsylvanian tidally influenced sediments from SW Indiana. Org. Geochem. 1999, 30, 1, 57–73.
24. Zhao, X.Q.; Chen, H.L.; Zhang, F.Q.; Sun, M.D.; Yang, J.G.; Tan, B.D. Characteristics, structural styles and tectonic implications of Mesozoic-Cenozoic faults in the eastern Heilongjiang basins (NE China). J. Asian Earth Sci. 2017, 146, 15, 196–210.
25. Shan, C.G.; Zhang, T.S.; Liang, X.; Zhang, Z.; Wang, M.; Zhang, K.; Zhu, H.H. On the fundamental difference of adsorption-pores systems between vitrinite- and inertinite-rich anthracite derived from the southern Sichuan basin, China. J. Nat. Gas. Sci. Eng. 2018, 53, 32-44.
26. Hou, H.H.; Shao, L.Y.; Li, Y.H.; Li, Z.; Wang, S.; Zhang, W.L.; Wang, X.T. Influence of coal petrology on methane adsorption capacity of the Middle Jurassic coal in the Yuqia Coalfield, northern Qaidam Basin, China. J. Pet. Sci. Eng. 2017, 149, 20, 218–227.
27. Cai, Y.D.; Li, Q.; Liu, D.M.; Zhou, Y.F.; Lv, D.W. Insights into matrix compressibility of coals by mercury intrusion porosimetry and N2 adsorption. Int. J. Coal. Geol. 2018, 200, 1, 199-212.
28. Zeng, F.H.; Peng, F.; Guo, J.C.; Wang, D.Y.; Zhang, S.R.; Zhang, P.; Zhang, B.; Gas transport study in the confined microfractures of coal reservoirs. J. Nat. Gas. Sci. Eng. 2019, 68, 102920.
29. Cai, Y.D.; Liu, D.M.; Pan, Z.J.; Che, Y.; Liu, Z.H. Investigating the Effects of Seepage-Pores and Fractures on Coal Permeability by Fractal Analysis. Transport. Porous. Med. 2016, 111, 479–497.
30. Zhao, J.L.; Xu, H. Tang, D.Z.; Mathews, J.P. Li, S.; Tao, S. Coal seam porosity and fracture heterogeneity of macrolithotypes in the Hancheng Block, eastern margin, Ordos Basin, China. Int. J. Coal Geol. 2016, 159, 1, 18-29.
31. Diessel, C.F.K. The correlation between coal facies and depositional environments, in: advances in the study of the Sydney Basin. Proceedings of 20th Symposium. The University of Newcastle, Newcastle, 1986, pp. 19–22.
32. Zhang, P.F.; Jin, K.L.; Wu, T.; Wang, C.G. Coal-bearing sedimentary and coal formed oil,Turpan-Hami basin. Coal Ind. Press. Beijing 1997, pp.168–176.
33. Janssen, C.; Wirth, R.; Reinicke, A.; Rybacki, E.; Naumann, R.; Wenk, H.-R.; Dresen, G. Nanoscale porosity in SAFOD core samples (San Andreas Fault). Earth Planet. Sci. Lett. 2011, 301, 179–189.
34. Khare, N.; Nigam, R.; Mayenkar, D.N.; Saraswat, R. Cluster analysis of benthic foraminiferal morpho-groups from the western margin of India reflects its depth preference. Cont. Shelf Res. 2017, 151, 72–83.

Peer-reviewed version available at *Energies* **2020**, *13*, 1196; doi:10.3390/en13051196

35. Peng, S.; Xiao, X.H. Investigation of multiphase fluid imbibition in shale through synchrotron-based dynamic micro-CT imaging. J. Geophys. Res. Solid Earth 2017, 122, 6, 4475–4491.
36. Zhang Y.H., Lebedev, M.; Sarmadicaleh, M.; Barifcani, A.; Rahman, T.; Lglauer, S.J. Swelling effect on coal micro structure and associated permeability reduction. Fuel. 2016, 182, 15, 568–576.
37. Mastalerz, M.; Drobniak, A.; Strąpoć, D.; Solano Acosta, W.; Rupp, J. Variations in pore characteristics in high volatile bituminous coals: Implications for coal bed gas content. Int. J. Coal Geol. 2008, 76, 205–216.